


Article

# A Dual Stable Isotope Approach Unravels Common Climate Signals and Species-Specific Responses to Environmental Change Stored in Multi-Century Tree-Ring Series from the Tibetan Plateau

Jussi Grießinger <sup>1,\*</sup>, Achim Bräuning <sup>1</sup>, Gerhard Helle <sup>2</sup>, Gerhard Hans Schleser <sup>3</sup>, Philipp Hochreuther <sup>1</sup> , Wolfgang Jens-Henrik Meier <sup>1</sup> and Haifeng Zhu <sup>4</sup>

<sup>1</sup> Institute of Geography, Friedrich-Alexander-University Erlangen-Nürnberg, 91058 Erlangen, Germany; achim.braeuning@fau.de (A.B.); philipp.hochreuther@fau.de (P.H.); wolfgang.jh.meier@fau.de (W.J.-H.M.)

<sup>2</sup> GFZ German Research Centre for Geoscience, Section 5.2 Climate Dynamics and Landscape Evolution, 14473 Potsdam, Germany; gerhard.helle@gfz-potsdam.de

<sup>3</sup> FZJ Research Centre Jülich, Institute of Bio- and Geosciences IBG-3, 52428 Jülich, Germany; g.schleser@fz-juelich.de

<sup>4</sup> Institute of Tibetan Plateau Research, Chinese Academy of Sciences, Beijing 100864, China; zhuhf@itpcas.ac.cn

\* Correspondence: jussi.griessinger@fau.de; Tel.: +49-9131-85-22009

Received: 13 February 2019; Accepted: 23 March 2019; Published: 29 March 2019



**Abstract:** Tree-rings are recorders of environmental signals and are therefore often used to reconstruct past environmental conditions. In this paper, we present four annually resolved, multi-centennial tree-ring isotope series from the southeastern Tibetan plateau. The investigation site, where juniper and spruce trees jointly occur, is one of the highest known tree-stands in the world. Tree ring cellulose oxygen ( $\delta^{18}\text{O}$ ) and carbon ( $\delta^{13}\text{C}$ ) isotopes were analyzed for a common period of 1685–2007 AD to investigate climate–isotope relationships. Therefore, various climate parameters from a local meteorological station and from the CRU 4.02 dataset were used. Tree-ring  $\delta^{18}\text{O}$  of both species revealed highly significant sensitivities with a high degree of coherence to hydroclimate variables during the growing season. The obtained  $\delta^{18}\text{O}$ –climate relationships can even be retained using a species mean. In contrast, the individual  $\delta^{13}\text{C}$  series indicated a weaker and non-uniform response to the tested variables. Underlying species-specific responses and adaptations to the long-term trend in atmospheric  $\text{CO}_2$  bias even after a trend correction identified dominant environmental factors triggering the tree-ring  $\delta^{13}\text{C}$  at our site. However, analysis of individual intrinsic water-use efficiency in juniper and spruce trees indicated a species-specific adaptation strategy to climate change.

**Keywords:** tree-ring  $\delta^{18}\text{O}$ ; tree-ring  $\delta^{13}\text{C}$ ; *Juniperus tibetica*; *Picea balfouriana*; Tibetan plateau; intrinsic water-use efficiency (iWUE); multi-centennial isotope time-series

## 1. Introduction

Often-quoted in a broader context as the “Third Pole” [1], an important part of the “Asian Water Towers” [2], or the “Roof of the World” [3], the Tibetan plateau (TP) exerts a key role for the climatic, hydrological and biological conditions of its highlands, mountain ranges as well as for the adjoining Asian lowland areas. Beyond the fact of its substantial role within the global climate system as the key driver of the Asian monsoonal systems [4], the current changes within the regional cryosphere, hydrosphere, biosphere and associated responses of environmental systems on the TP are subjects of intensive research. Especially, the responses, threats and adaptations of different (socio-)ecosystems

to the substantial rise in temperature during the recent decades and associated changes of water availability underline the necessity of a precise quantification of these changes [5–9]. Contrastingly, for High Asia in general and for the Tibetan plateau in particular, only a sparse climate station network with relatively short time-series of high-resolution meteorological data is available. Therefore, existing datasets, which are mainly available at the earliest since the 1950s, hamper a substantial quantification and classification of the recent climate change within a retrospective context and underline the needs for paleoclimatic datasets [4,10–12].

Besides studies focusing on tree-ring width (TRW), more and more studies display the advantages of using stable isotopes in tree-rings for ecological as well as paleoclimate research on the Tibetan plateau. During the last decade, the analysis and use of tree-ring  $\delta^{18}\text{O}$  has become one of the main proxies used for paleoclimate research in High Asia. Recent works on the Tibetan Plateau, in particular, have demonstrably contributed to a better understanding of regional climate and environmental history [10–17]. In comparison, studies on the  $\delta^{13}\text{C}$  variations in tree-rings are still underrepresented due to more complex isotope fractionation effects affecting the  $\delta^{13}\text{C}$  in tree-rings. In addition, multi-century  $\delta^{13}\text{C}$  tree-ring time series usually have to undergo a trend correction procedure primarily due to the rising atmospheric  $\text{CO}_2$  concentrations ( $\text{CO}_2_{\text{ATM}}$ ) since the beginning of the industrialization (the “Suess-effect”). Especially the respective correction factor that has to be considered due to plant-internal reactions addressing rising  $\text{CO}_2_{\text{ATM}}$  has considerable impact on the adjustment of carbon isotope time series [18,19] and may strongly modify trends of  $\delta^{13}\text{C}$  tree-ring data after correction.

Recently, progress has been made in studies on analyzing both stable carbon and oxygen isotopes, pointing to the paleoclimatic potential inherent to such an approach [20–23]. In addition, studies underline the potential and benefit within the analysis of multiple stable isotopes across species and across sites [24,25]. The reported advantage is mainly based on the possibility of a common assessment and interpretation of stored climate signals with coupled ecophysiological reactions across tree species. However, up to now, the mentioned studies focus either on the analysis of two tree species, but only for over a rather short time period of a few decades, or the establishment of longer (multi-century to millennial) time series for two isotopes, but only investigating a single tree species. The main reason for this desideratum is presumably caused by the comparably high laboratory and time expenditure inherent to tree-ring isotope studies, although many sites on the TP possibly bear the potential of additionally analyzing several tree species. For a profound retrospective assessment, classification and categorization of the recently ongoing environmental changes and tree-specific adaptations, longer isotope time-series across species are, however, urgently required.

When considering existing studies on tree-ring  $\delta^{13}\text{C}$  and  $\delta^{18}\text{O}$  from the TP, their spatial representativity and probable inter-isotope dependencies sometimes remain difficult. Due to the lack of other existing, closely situated tree-ring isotope series especially for carbon isotope series, it remains often challenging to corroborate a wider regional representativity. Moreover, the derived, detected and stored environmental signal in the tree-ring proxy is reported to reflect a more site- and species-related physiological response to the ongoing environmental change [26,27]. This includes in particular observed adaptations in different tree species with regard to changes in their intrinsic water-use efficiency [25,28]. The sometimes heterogeneous picture with regard to the (reconstructed) environmental signal stored in  $\delta^{13}\text{C}$  and  $\delta^{18}\text{O}$  series from the TP, the different levels in signal strength and differing spatial representativities of the time series still contain challenges for actual and future research.

By analyzing multi-centennial variations of different stable isotopes ( $\delta^{13}\text{C}$  and  $\delta^{18}\text{O}$ ) in two different tree species from a common site on the southeastern part of the TP, our study evaluated the potential, benefit, and limitations inherent in such an approach by:

- (i) deciphering and explaining common and contrasting long-term isotopic variations of  $\delta^{13}\text{C}$  and  $\delta^{18}\text{O}$  between two tree species from high-altitude, climate-sensitive tree-stands;
- (ii) assessing the added value for an analysis of  $\delta^{13}\text{C}$  and  $\delta^{18}\text{O}$  from two local tree species; and

- (iii) testing if common/differing signals of the proxy series from one site can be used to better assess, decipher, and explain diverging responses of tree species to recent environmental change.

The main aim of this study was therefore a calibration study on the potential of multiple isotope parameters derived from tree-rings from a subalpine tree-stand in High Asia.

## 2. Materials and Methods

### 2.1. Study Site

The study site is situated around 20 km southwest to the municipality of Qamdo on the upper reaches of the Mekong River on the southeastern Tibetan plateau (TP) (Figure 1). The local climate as recorded by the nearby climate station in the municipality of Qamdo (31°09' N/97°10' E; available period 1954–2012) is characterized by a mean annual temperature of 8.8 °C and an annual precipitation sum of 482 mm, indicating a sub-humid continental climate (Figure 1). The main summer season lasts from June to August and represents the period with highest temperatures ( $T_{JJA} = 16.7$  °C). Summer months with the maximum monthly temperatures are July ( $T_{July} = 17.4$  °C) and August ( $T_{Aug} = 16.6$  °C), respectively. The summer months July and August have the highest amounts of precipitation ( $Precip_{JJA} = 296$  mm;  $Precip_{July} = 107$  mm,  $Precip_{Aug} = 101$  mm). In contrast, winter months are cold and show little to no rainfall/snow ( $T_{Dec} = 0$  °C,  $Precip_{Dec} = 2$  mm). Overall, local climate conditions display a typical summer monsoon climate with warm and humid summers contrasted by cold and dry winter conditions [4].

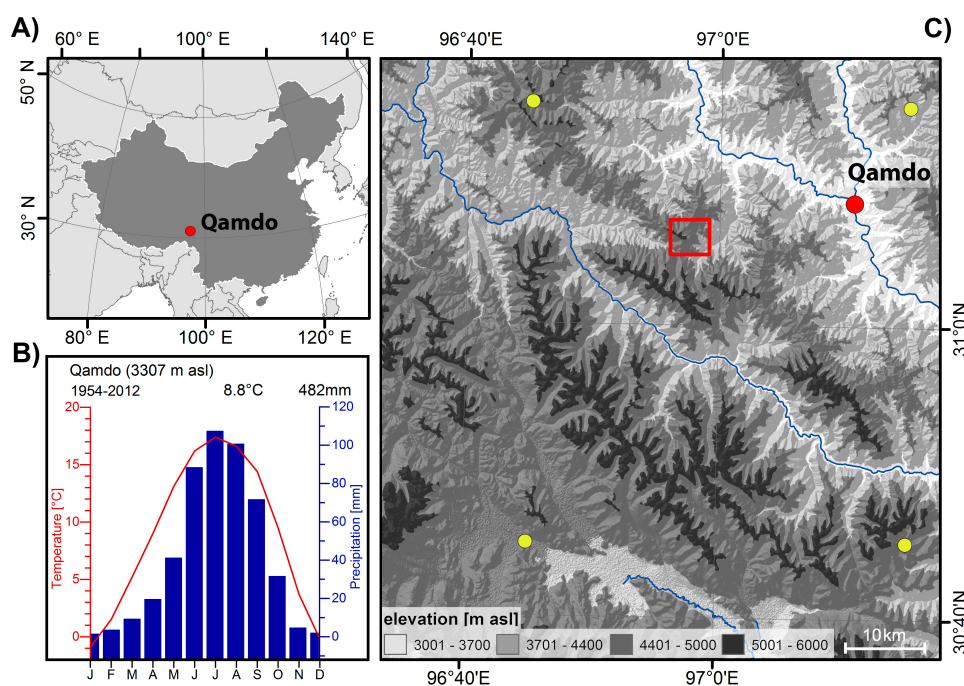


**Figure 1.** Overview of the investigation site: (A) location of the site Qamdo within China; (B) climate diagram of the climate station in Qamdo; and (C) digital elevation map of the Qamdo region with the investigation site (red box), location of the city and climate station of Qamdo (red dot). Yellow points indicate locations of the used 0.5° CRU TS 4.02 grid points.

The investigated tree-stand is located at the local subalpine vegetation belt between 4400 m and 4600 m asl. on a convex slope with slightly changing southerly expositions (Figure 2). Developed from debris material, predominant soils are well-drained and shallow without influence of stagnating groundwater [12,29,30]. The upper timberline on southerly exposed slopes is formed by open, steppe-forest-like formations of Tibetan juniper (*Juniperus tibetica* Kom.), being one of the highest

known tree-stands of the world at 4600 m asl. [31]. On average, juniper tree individuals reach heights of up to 12 m, with some individuals exceeding 20 m. As being typical for steppe forests, the juniper tree stand is characterized by a canopy cover of 10%. On eastern and southeastern expositions, denser stands of 20–25 m high Balfour spruce trees (*Picea balfouriana*) with a canopy cover of maximum 25% are dominant, reaching their maximum upper distribution limit at 4500 m asl. In contrast to the juniper stands, spruce trees are in parts covered with lichens of the species *Alectoriella ssp.*, pointing to more humid microclimatic conditions presumably caused by lower radiation and higher humidity (cf. Figure 2).



**Figure 2.** Overview on the sampling site near Qamdo: (I) area of predominant *Juniperus tibetica* tree-stands on southerly expositions at 4400–4600 m asl.; and (II) vegetation belt with the *Picea balfouriana* forest on southeasterly expositions.

## 2.2. Sampling, Dating and Sample Preparation

During several field campaigns, undisturbed and healthy mature tree-individuals of *Picea* and *Juniperus* species were sampled. We collected discs from dead trees and increment cores from living trees using an increment borer (Suunto). In the laboratory, samples were surfaced and tree ring widths were measured with an accuracy of 0.01 mm using a Lintab 6 system (Rinntech, Heidelberg/Germany). Subsequently, samples were cross-dated and validated against an existing regional master chronology [29,30]. For the analysis of the ratios of stable oxygen and carbon isotopes from tree-ring cellulose (thereafter expressed as  $\delta^{18}\text{O}_{\text{TRC}}$  and  $\delta^{13}\text{C}_{\text{TRC}}$ ), at least 5–7 cores from both juniper and spruce individuals were selected. The obtained minimum sample depth of five trees was within the generally accepted threshold of analyzed trees per species per sample site for isotope studies [32] and was consistently available throughout the common period 1685–2007 AD covered by both species (Table 1).

**Table 1.** General site information and chronology statistics for the common period 1685–2007.

Species	Altitude (m asl.)	Chronology Time Span	Mean $\delta^{18}\text{O}_{\text{TRC}}$	Mean $\delta^{13}\text{C}_{\text{TRC}}$ Corrected	SD	AC1
<i>Juniperus tibetica</i>	4600 m	489–2011 AD	23.33‰	−20.46‰	1.2 ( $\delta^{18}\text{O}$ ) 0.5 ( $\delta^{13}\text{C}$ corr.)	0.61 ( $\delta^{18}\text{O}$ ) 0.74 ( $\delta^{13}\text{C}$ corr.)
<i>Picea balfouriana</i>	4400 m	1685–2007 AD	22.98‰	−20.67‰	1.4 ( $\delta^{18}\text{O}$ ) 0.9 ( $\delta^{13}\text{C}$ corr.)	0.26 ( $\delta^{18}\text{O}$ ) 0.81 ( $\delta^{13}\text{C}$ corr.)

All samples chosen for isotope analysis met the following criteria: (i) similar tree ages for juniper and spruce trees; (ii) no missing rings or occurrence of problematic plateaus with extremely depressed growth and narrow rings to obtain sufficient  $\alpha$ -cellulose for the analysis of both  $\delta^{13}\text{C}_{\text{TRC}}$  and  $\delta^{18}\text{O}_{\text{TRC}}$ ; and (iii) the analytical exclusion of the innermost 50 years of each sample to avoid a non-climatic juvenile trend of the most recent  $\delta^{13}\text{C}_{\text{TRC}}$  values [33]. Especially Criterion (ii) was difficult to meet within multi-century old junipers known for lobate growth and in parts extremely narrow ring widths [11,12]. To obtain sufficient material for the analysis of both isotopes from such samples, it was therefore inevitable to pool material of corresponding calendar years prior to the subsequent laboratory steps, as reported and successfully applied within existing studies [11–14,17,32,33]. To avoid a mass-related over-representation of a single tree individual within our pooled samples, cut wood samples of every tree-ring were weighed individually prior to cellulose extraction. Subsequently, same amounts of each calendar year were combined for the final pooled sample year. In regard to the aim of this study of an inter tree-species comparison with the precondition of a comparable analytical setting and subsequent sound statistical analyses, sample pooling was also performed for the spruce samples.

### 2.3. Evaluation of $\delta^{18}\text{O}_{\text{TRC}}$ and $\delta^{13}\text{C}_{\text{TRC}}$

In a first analytical step, dated growth rings of both species were cut under a binocular using a razor blade. Calendar year-wise pooled wholewood samples of juniper and spruce were processed to  $\alpha$ -cellulose following the method in [34]. After the extraction process, the obtained cellulose samples were homogenized using an ultrasonic sound system and finally freeze-dried in a lyophilization unit [35]. Cellulose samples of each species of 200  $\mu\text{g}$  were weighed using a micro balance and individually packed in tin (for carbon isotope analyses) and silver capsules (for oxygen isotope analyses), respectively. Measurements of the  $^{12}\text{C}/^{13}\text{C}$  ratio (expressed as  $\delta^{13}\text{C}$ ) and  $^{16}\text{O}/^{18}\text{O}$  ratios (expressed as  $\delta^{18}\text{O}$ ) of spruce and juniper samples were determined using a continuous flow DELTA V Advantage Isotope Ratio Mass Spectrometer (IRMS, Thermo Fisher Scientific Inc.) (Waltham, MA, USA). To avoid a hygroscopically caused exchange with ambient air, all samples for the assessment of oxygen analyses were stored prior to the IRMS analysis for at least 48 hours in a vacuum oven.

For the analysis of  $\delta^{18}\text{O}_{\text{TRC}}$  isotopes, samples were pyrolyzed to CO in a HEKATech pyrolysis reactor coupled to the IRMS at 1080 °C. For the measurements of the  $\delta^{13}\text{C}$  variations in tree-ring cellulose, samples were combusted at 1020 °C under an excess of oxygen to CO<sub>2</sub>. All measurements were calibrated by periodically interposing internal and international laboratory standards resulting in an overall analytical precision for the  $\delta^{18}\text{O}_{\text{TRC}}$  measurements of <0.2‰ and for the  $\delta^{13}\text{C}_{\text{TRC}}$  measurements of <0.1‰, respectively.

As a result, we were able to set up for both investigated stable isotopes juniper chronologies with periods reaching from 489 to 2011 AD. At this point, it has to be noted that the *Juniperus*  $\delta^{18}\text{O}_{\text{TRC}}$  time series was already used for a climate reconstruction [12]. However, by using new material, we were able to update the series until 2011 AD. Thereto, pooled samples of the new individuals were analyzed with an overlap of 20 years to the existing series. Due to their lower maximal biological age, the obtained spruce isotope chronologies cover the period from 1685 to 2007 AD. Hence, the common and further considered period covered by both species lasts from 1685 to 2007 AD.

### 2.4. Examination of Isotope–Climate Relationships

As being a crucial step for the calibration of tree-ring proxy data in remote high elevation areas, we conducted a thorough survey of available and representative climate datasets. For a first examination of climate–proxy relationships, instrumental data from the nearby climate station in Qamdo (available since 1954) were used. The dataset includes a wide variety of climate parameters including precipitation, temperature ( $T_{\text{min}}$ ,  $T_{\text{max}}$ , and  $T_{\text{mean}}$ ), wind speed (ws), vapor pressure deficit (vp), sunshine hours (sh), and relative humidity (rH). Especially in high mountain areas such as the TP with steep topoclimatic gradients within short distances, precipitation data from climate stations located in valley bottoms often show a limited representativity for study sites located at the upper tree

line. Therefore we additionally used gridded means of climate variables from the four nearest 0.5° grid points of the CRU TS 4.02 dataset (Figure 1; [https://crudata.uea.ac.uk/cru/data/hrg/cru\\_ts\\_4.02/cru\\_ts.1811131722.v4.02/](https://crudata.uea.ac.uk/cru/data/hrg/cru_ts_4.02/cru_ts.1811131722.v4.02/)) [36]. Therein, provided climate parameters are precipitation, temperature ( $T_{\max}$ ,  $T_{\text{mean}}$ , and  $T_{\min}$ ), diurnal temperature range (dtr), wet day frequencies (wet), cloud cover (cld), frost day frequency (frs), and potential evapotranspiration (pet). When using gridded datasets from this area, however, it must always be taken into account that the early periods are interpolated from a rather low number of available climate stations. Therefore, we truncated the first five decades and only used the CRU data for the common period with stationary data for 1954–2007 ( $n = 53$ ) where highly significant relationships between both datasets appear ( $p < 0.01$ ).

For the quantification of the statistical relationships, we computed Pearson's correlation coefficients ( $r$ ) for all available variables in both datasets. The resultant correlations are visualized in a correlogram [37] where correlation coefficients are colored according to their positive/negative value including the respective level of significance. To determine the influence of the applied CO<sub>2</sub> trend correction on the correlations with climate, time series of all isotopes and tree species were filtered using a multiple local regression filter with windows set to 1/10 of the time series length. Wavelet analysis was employed to explore the existence and significance of high- and low-frequency dynamics and the threshold for the high-pass filter (R package WaveletComp). Running correlations for all isotopes and tree species were computed using a 50-year moving window.

### 2.5. $\delta^{13}\text{C}_{\text{TRC}}$ Detrending and *iWUE* Calculation

As reported by many other studies,  $\delta^{13}\text{C}_{\text{TRC}}$  time-series are often characterized by a significant decreasing trend. This decline is mainly caused by the steadily increasing combustion of fossil fuels since the beginning of the industrialization after ca. 1850 AD [18,33]. As a result, the absolute amount of the atmospheric CO<sub>2</sub> concentration has risen steadily since 1800 from 270 ppm up to presently 410 ppm ([38], <https://www.esrl.noaa.gov/gmd/ccgg/trends/data.html>). Through primarily released lighter <sup>12</sup>C isotopes, fossil fuel combustion has led to a coupled shift in the atmospheric <sup>12</sup>CO<sub>2</sub>/<sup>13</sup>CO<sub>2</sub> relationship resulting in a depletion of the atmospheric  $\delta^{13}\text{CO}_2$  values. As a result, plants have and do still respond with plant physiological responses to the increased atmospheric CO<sub>2</sub> which in turn are biasing the environmental signals stored in tree-ring cellulose [19,32]. To minimize this anthropogenic bias and to extract the environmental signal incorporated within the  $\delta^{13}\text{C}_{\text{TRC}}$ , a trend-correction of the  $\delta^{13}\text{C}_{\text{TRC}}$  raw values has to be performed prior to the assessment of climate- $\delta^{13}\text{C}_{\text{TRC}}$ -relationships. Within our study, we used the rather conservative non-linear  $\delta^{13}\text{C}$ -trend correction for CO<sub>2</sub> ATM, as introduced in [18].

To initially test a possible individual response of our two studied tree species towards changing CO<sub>2</sub> concentrations, we calculated for the period 1900–2007 their respective intrinsic water-use efficiencies (*iWUE*). As reported in [39], the *iWUE* is defined as the ratio of net photosynthetic assimilation rate ( $A$ ) to stomatal conductance ( $g_s$ ) for water vapor. It is calculated as:

$$iWUE = A/g_s = C_a \times [(1 - C_i/C_a)/1.6], \quad (1)$$

where  $C_i$  and  $C_a$  are the CO<sub>2</sub> concentrations in the intercellular air space of the leaves and in the atmosphere, respectively.  $C_i$  can be obtained by calculating the carbon isotope discrimination ( $\Delta$ ) for C3 plants, as introduced in [40]. The  $\Delta$  is expressed therein as

$$\Delta = (\delta^{13}\text{C}_a - \delta^{13}\text{C}_p)/(1 + [\delta^{13}\text{C}_p/1000]), \quad (2)$$

where  $\delta^{13}\text{C}_a$  is the stable isotope value of the ambient air (in ‰) and  $\delta^{13}\text{C}_p$  the stable isotope value of plant cellulose (in ‰). Values for  $\delta^{13}\text{C}_a$  (including  $C_a$ ) for the period 1900–2007 were derived from the datasets in [18,28]; the respective  $\delta^{13}\text{C}_p$  denote the measured  $\delta^{13}\text{C}_{\text{TRC}}$  values from our study.

Since  $\Delta$  is also a function of the difference between the intercellular and the atmospheric  $\text{CO}_2$ , it can be additionally calculated as:

$$\Delta = a + (b - a) \times (C_i/C_a), \quad (3)$$

where  $a$  reflects the isotopic discrimination during diffusion of  $\text{CO}_2$  from the atmosphere into the intercellular space ( $\sim 4.4\%$ ), and  $b$  denotes the isotopic discrimination caused by the discrimination against  $\text{CO}_2$  in the chloroplasts by the enzyme RuBisCO ( $\sim 27\%$ ).

### 3. Results and Discussion

#### 3.1. Species Specific Characteristics of $\delta^{18}\text{O}_{\text{TRC}}$

Figure 3 shows the resulting  $\delta^{18}\text{O}_{\text{TRC}}$  time series of the two studied tree species at Qamdo during 1685–2007. For a better comparability of the low-frequency variations between the  $\delta^{18}\text{O}_{\text{TRC}}$  time series, the scale of the individual series was adjusted by an offset of  $4\%$ . A first quantitative examination of the two time-series already reveals a high visual similarity (Table 2). The mean values of the oxygen isotope series differ slightly within a range of about  $0.6\%$  ( $\delta^{18}\text{O}_{\text{TRC Juniper}} = 23.43\%$ ,  $\delta^{18}\text{O}_{\text{TRC Spruce}} = 22.98\%$ ). Since both tree-species are situated within a short elevational range, this is assumed to be caused by slightly different plant-internal fractionations during cellulose synthesis and/or—on a microclimatic scale—a slightly differing moisture availability during the vegetation period. Probably caused by a higher proportion of earlywood [11,12], the juniper chronology is characterized by a higher autocorrelation ( $\text{AC1} = 0.61$ ) than the spruce time-series ( $\text{AC1} = 0.26$ ). It is apparent that the inter-annual variability of the individual time-series is considerably high (Figure 3). In particular, during the recent decades, the number of positive and negative excursions in both time series exceeding a deviation of more than  $1.5$  SD increased compared to their long-term mean.

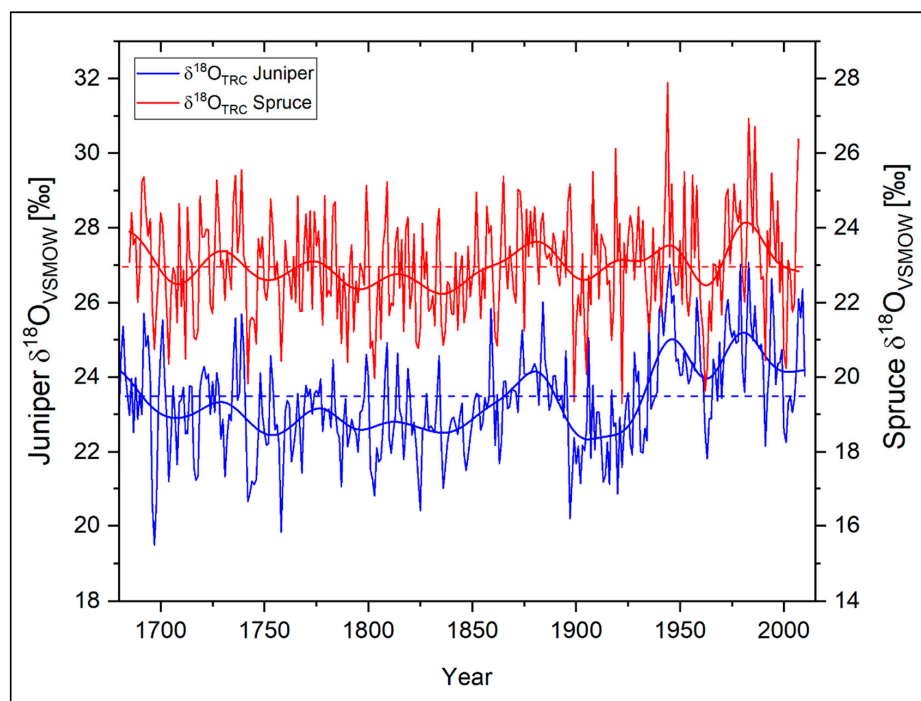


**Figure 3.** Annual  $\delta^{18}\text{O}_{\text{TRC}}$  variations of *Juniperus tibetica* (blue) and *Picea balfouriana* (red) at Qamdo for the period 1685–2010. Bold lines represent the respective 11-year Fast Fourier Transform (FFT) filter for each time-series, dotted horizontal lines the individual species mean. Note: Individual y-axes are shifted against each other with an offset of  $4\%$  to better show the high synchronicity between both time-series.

The highly significant ( $p < 0.01$ ) correlation coefficient of  $r = 0.60$  and Gleichläufigkeit (sign test) of 70% between the isotope chronologies underline their strong common signal (Table 2). The similarity between the series is also shown by highly consistent variations on lower frequencies (11-year and 21-year Fast Fourier Transform (FFT) filter). While regarding the respective low frequency domains of the two series, the statistical relationships are even higher and stable within their respective levels of significance with  $p < 0.01$  (11-year FFT filtered:  $r = 0.73$ , GLK = 91%; 21-year FFT filtered:  $r = 0.75$ , GLK 78%). This leads to the assumption that both species are probably controlled by the same environmental influences and therefore show a very similar temporal variability and environmental sensitivity.

**Table 2.** Correlation coefficients ( $r$ ) and Gleichläufigkeit (GLK) between stable carbon and oxygen isotope time-series of *Juniperus tibetica* and *Picea balfouriana* on different frequency scales for the common period 1685–2007. All given values are highly significant at  $p < 0.01$ .

Stable Isotope Series	Annual	Low-Freq. (11-year FFT)	Low-Freq. (21-year FFT)
$\delta^{18}\text{O}_{\text{TRC}}$	$r = 0.60$ GLK = 70%	$r = 0.73$ GLK = 91%	$r = 0.75$ GLK = 78%
$\delta^{13}\text{C}_{\text{TRC raw}}$	$r = 0.86$ GLK = 51%	$r = 0.95$ GLK = 63%	$r = 0.96$ GLK = 63%
$\delta^{13}\text{C}_{\text{TRC CO}_2\text{-corr.}}$	$r = 0.44$ GLK = 52%	$r = 0.64$ GLK = 64%	$r = 0.69$ GLK = 65%

### 3.2. Species Specific Characteristics of $\delta^{13}\text{C}_{\text{TRC}}$

In contrast to the  $\delta^{18}\text{O}_{\text{TRC}}$ -variations, the courses of the  $\delta^{13}\text{C}_{\text{TRC}}$  time series highly differ between species. In general, both time series show an offset of around 2‰ in their individual mean values (mean  $\delta^{13}\text{C}_{\text{TRC juniper}} = -18.83\text{‰}$ , mean  $\delta^{13}\text{C}_{\text{TRC spruce}} = -20.92\text{‰}$ ). Mainly caused by the steadily rising influence of  $^{13}\text{C}$ -depleted atmospheric  $\text{CO}_2$ , both series are highly influenced by a markedly negative trend since the end of the 19th century. After 1900 AD, this anthropogenic trend becomes more apparent for the juniper trees, resulting in an absolute minimum of the  $\delta^{13}\text{C}_{\text{TRC juniper}}$  series in 2010 at  $-21.59\text{‰}$  (Figure 4). For the spruce trees, a corresponding trend can be observed, resulting in the lowest overall value of  $-24.21\text{‰}$  in 2005. As mentioned, this non-climatic trend has to be corrected before evaluating the respective climate–proxy relationship. Figure 4 displays the results of the performed  $\delta^{13}\text{C}$  trend correction on the two isotope chronologies. By regarding the common period (1685–2007) of both  $\text{CO}_2$ -corrected time series, it is noticeable that both tree species exhibit an overall negative trend (Figure 4), which is more prominent for spruce. During the pre-industrial period, long-term linear trends in both species display a similar, only slightly negative trend. After 1850, these trends are further enhanced with different timing and magnitude between the species. Compared to the juniper trees, the linear long-term trend of spruce  $\delta^{13}\text{C}_{\text{TRC}}$  indicate a more pronounced decrease after 1850 AD. While regarding the 11-year FFT filter of both species (Figure 4), this can be explained by an apparent positive trend in the juniper  $\delta^{13}\text{C}_{\text{TRC}}$  until the early 20th century. Thereafter, the junipers also show a comparable negative trend to the absolute minimum of the time series in 2007. Presumably, these differing trends point to species-specific physiological strategies against the rising atmospheric  $\text{CO}_2$  content.



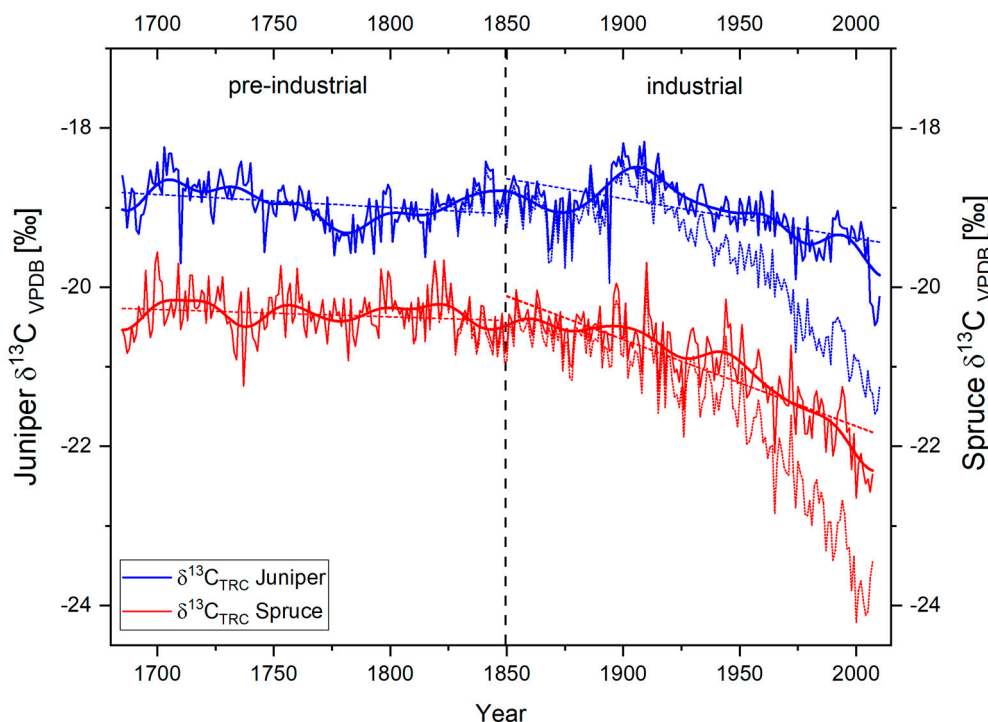


**Figure 4.** Annual  $\delta^{13}\text{C}_{\text{TRC}}$  variations of *Juniperus tibetica* (blue) and *Picea balfouriana* (red) at Qamdo for the period 1685–2011. Bold lines represent  $\delta^{13}\text{C}_{\text{TRC}}$   $\text{CO}_2$ -corrected series and associated 11-year Fast Fourier Transform (FFT) filters, bright dotted time series indicate the species specific uncorrected  $\delta^{13}\text{C}_{\text{TRC}}$  raw series, and dotted lines represent species-specific linear trends of the corrected  $\delta^{13}\text{C}_{\text{TRC}}$  series over the pre-industrial (1685–1849) and industrial period (1850–2007), respectively.

Compared to the  $\delta^{18}\text{O}_{\text{TRC}}$  time-series, the correlation between the species-specific corrected  $\delta^{13}\text{C}_{\text{TRC}}$  chronologies is lower ( $r = 0.44$ ,  $\text{GLK} = 52\%$ ; Table 2). Although the statistical interrelation increases in the low frequency domains (11-year FFT filtered:  $r = 0.64$ ,  $\text{GLK} = 64\%$ ; 21-year FFT filtered:  $r = 0.69$ ,  $\text{GLK} = 65\%$ ), this is assumable mainly caused by—despite the applied  $\text{CO}_2$ -correction—the still apparent negative trend since 1800 AD. The high influence and species-specific bias of this trend is additionally displayed in Table 2 by calculations with the uncorrected  $\delta^{13}\text{C}_{\text{TRC}}$  raw values.

### 3.3. Climate– $\delta^{18}\text{O}_{\text{TRC}}$ Relationships

The climate–isotope relationships for the two investigated tree species based on calculations with the climate station at Qamdo are displayed in the Figure 5A,B. According to the high similarity between the  $\delta^{18}\text{O}_{\text{TRC}}$ -series of both species, it was expected that the resulting climate correlations are highly synchronous. To check the potential benefit and additional information inherent in a combination of tree species, we tested the applicability of a mean isotope series. To evaluate if the climate signal is dominant over species-specific plant-physiological growth characteristics, juniper and spruce  $\delta^{18}\text{O}_{\text{TRC}}$  chronologies were averaged. Additionally, the first principal components (PC) of the two tree species for both isotopes were computed, with prior centering and scaling applied, as  $\delta^{13}\text{C}_{\text{TRC}}$  values differ significantly in their mean. Since for two centered and standardized variables, the correlation matrix always has the same eigenvectors, the correlation between its first PC and the mean is 1. Therefore, we used the calculated species  $\delta^{18}\text{O}_{\text{TRC}}$  mean and performed the same correlation analyses as for the individual species (Figure 5C).

It is apparent that hydroclimatic parameters including precipitation, vapor pressure deficit and relative humidity (rH) have the highest negative influence on the  $\delta^{18}\text{O}$  variations in spruce and juniper tree-rings. Values of juniper  $\delta^{18}\text{O}_{\text{TRC}}$  reveal highly significant correlations with different monthly and seasonal means during the vegetation period (lasting from May to September) of different

hydroclimatic variables (Figure 5A). Within those, correlations with relative humidity averaged over the complete vegetation period have the strongest (negative) impact on  $\delta^{18}\text{O}_{\text{TRC}}$  ( $r_{\text{MJJAS}} = -0.67$ ,  $p < 0.01$ ). Considering the high autocorrelation of the juniper  $\delta^{18}\text{O}_{\text{TRC}}$  series, the implementation of the previous year’s vegetation period even slightly increases correlations with rH ( $r_{\text{MJJAS} + \text{pyMJJAS}} = -0.68$ ,  $p < 0.01$ ). Precipitation ( $r_{\text{precip MJJAS}} = -0.46$ ,  $p > 0.01$ ), nd vapor pressure ( $r_{\text{MJJAS}} = -0.59$ ,  $p < 0.01$ ) are also significantly correlated to  $\delta^{18}\text{O}_{\text{TRC}}$  during the summer season. Positive significant correlations occur with maximum temperature during May to September ( $r_{\text{MJJAS}} = 0.45$ ,  $p < 0.01$ ). Results for single months display similar sensitivities, although showing continuously lower correlation strength.

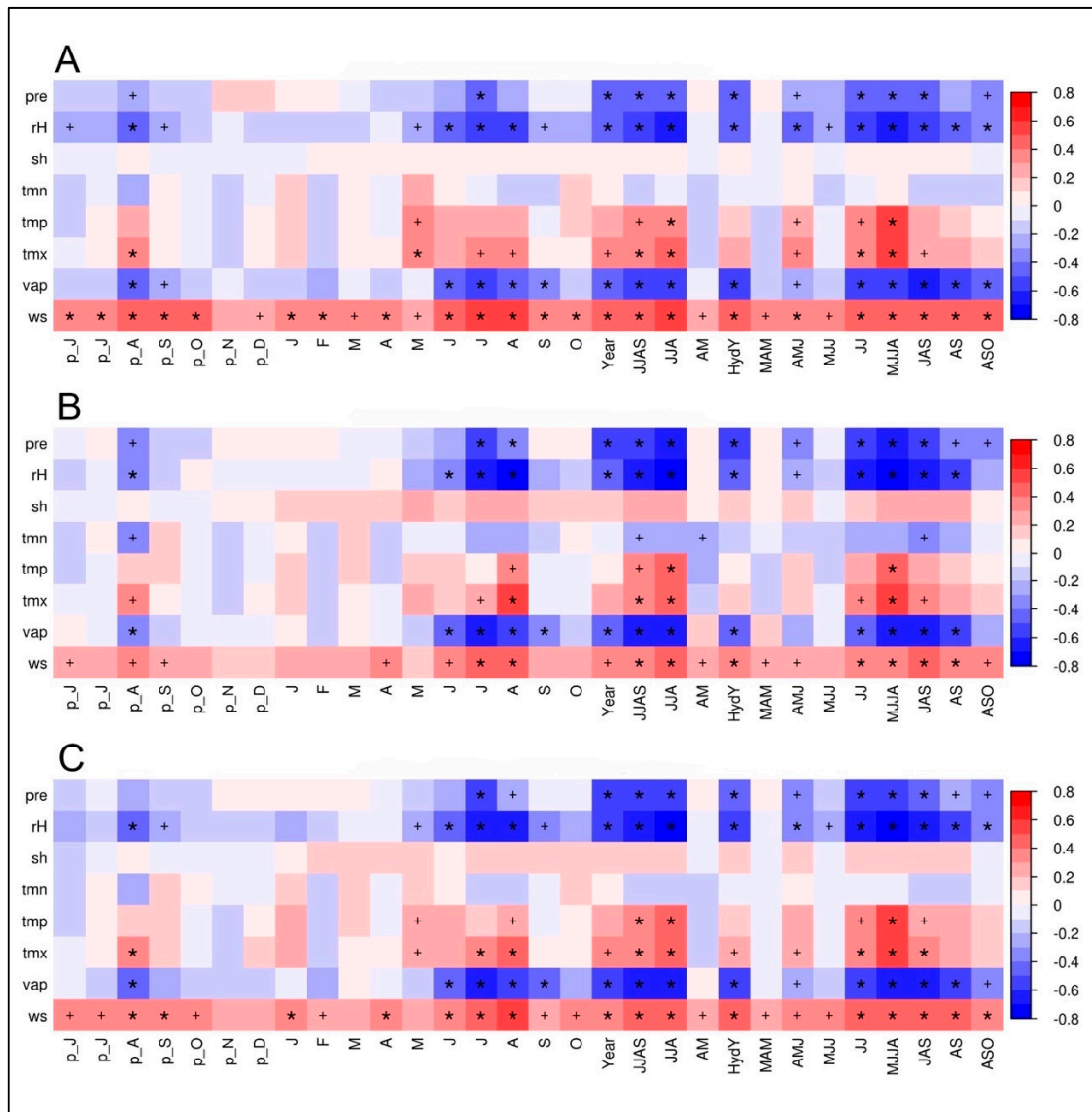


**Figure 5.** Climate–proxy relationships between  $\delta^{18}\text{O}_{\text{TRC}}$  of: juniper trees (A); spruce trees (B); and the site-internal  $\delta^{18}\text{O}_{\text{TRC}}$  mean (C) plotted against monthly and seasonal averages of different climate parameters (pre, precipitation; rH, relative humidity; sh, sunshine hours; tmn, minimum temperature; tmp, mean temperature; tmx, maximum temperature; vap, vapor pressure deficit; ws, wind speed) from Qamdo climate station for the period 1954–2007 ( $n = 54$ ). The prefix “p” indicates relationships to the previous years’ monthly means. Red/blue colors indicate positive/negative correlation coefficients ( $r$ ). The respective level of significance is displayed by a plus sign ( $p < 0.05$ ) or an asterisk ( $p < 0.01$ ).

Nearly identical climate–proxy relationships are apparent for spruce and the Qamdo climate station (Figure 5B). The corresponding correlogram reveals nearly the same pattern as for juniper,

although the individual absolute values of the correlations are mostly higher. Highly significant relationships occur with relative humidity and vapor pressure deficit during the summer months (rH:  $r_{\text{MJJJA}} = -0.74$ ,  $p < 0.01$ , vp:  $r_{\text{MJJJA}} = -0.62$ ,  $p < 0.01$ ), precipitation during the summer monsoon season ( $r_{\text{JJJA}} = -0.62$ ,  $p < 0.01$ ), and maximum temperatures in August ( $r_{\text{Aug}} = 0.52$ ,  $p < 0.01$ ). It is apparent that the hydroclimatic conditions during the vegetation period are decisive for the  $\delta^{18}\text{O}_{\text{TRC}}$  variations in the tree-ring.

The combined species' mean chronology showed largely identical results as displayed for the individual species' correlations (Figure 5C). Interestingly, statistical relationships and significance levels mainly represent mainly the levels of the results from the spruce trees (e.g., rH:  $r_{\text{MJJJA}} = -0.74$ ; vp:  $r_{\text{MJJJA}} = -0.62$ ,  $p < 0.01$ ), or are even increase in contrast to the species-specific results (rH:  $r_{\text{JJJA}} = -0.75$ ,  $p < 0.01$ ). The climate–isotope relationships are kept stable within such a combination of inter-species  $\delta^{18}\text{O}_{\text{TRC}}$  series, clearly indicating the strong influence of the same external/climate factor(s) on both species. This result underlines the use of an inter-species approach for using  $\delta^{18}\text{O}_{\text{TRC}}$  to reconstruct past climate variability and enhancing the representativity of tree-sites.

Proxy–climate calculations with climate variables from the CRU dataset also reflect the proposed general high similarities of responses among species (Figure S1). Interestingly, differences occur concerning the respective parameter and season the investigated species react most sensitive. Whereas the juniper  $\delta^{18}\text{O}_{\text{TRC}}$  is highly sensitive to climate parameters related to drought or moisture stress during the summer monsoon period (pet:  $r_{\text{MJJJA}} = -0.54$ ,  $p < 0.01$ ,  $T_{\text{Max}}$ :  $r_{\text{MJJJA}} = -0.51$ ,  $p < 0.01$ , precipitation  $r_{\text{MJJJA}} = 0.53$ ,  $p < 0.01$ ), spruce  $\delta^{18}\text{O}_{\text{TRC}}$  is more related to precipitation variations ( $r_{\text{MJJJA}} = -0.71$ ,  $p < 0.01$ ). Especially for the junipers, the location on a southerly exposed slope results in a more drought and insolation related sensitivity. In general, the correlations for junipers are more consistent than those of the spruce trees (Figure S1A,B). Presumably, the CRU dataset: (i) better reflects climate conditions at the upper tree-line; and (ii) is more representative for juniper than for spruce.

The assessment of the CRU– $\delta^{18}\text{O}_{\text{TRC}}$  relationship with a species' mean exceeds the already strong results revealed with local instrumental climate data. It is obvious that, by using a species' mean  $\delta^{18}\text{O}_{\text{TRC}}$  value, the species-specific correlations coefficients can be further increased (Figure S1C). For example, the correlation with potential evapotranspiration during the summer season (May to August) increases up to an r-value of  $r_{\text{MJJJA}} = 0.60$  ( $p < 0.01$ ), while species-specific results are noticeably lower (pet juniper:  $r_{\text{MJJJA}} = 0.50$ ; pet spruce:  $r_{\text{MJJJA}} = 0.54$ ). Similar effects can be obtained for maximum temperature during the same season, with a species-mean r-value of  $r_{\text{MJJJA}} = 0.52$  in comparison to the  $\delta^{18}\text{O}_{\text{TRC}}$  of juniper ( $r_{\text{MJJJA}} = 0.50$ ,  $p < 0.01$ ) or spruce ( $r_{\text{MJJJA}} = 0.47$ ,  $p < 0.01$ ). Apparently, by averaging the  $\delta^{18}\text{O}_{\text{TRC}}$  values of individual species, biases within the  $\delta^{18}\text{O}_{\text{TRC}}$  variations related to species-specific responses are dampened in favor to a common site signal.

### 3.4. Climate– $\delta^{13}\text{C}_{\text{TRC}}$ Relationships

As expectable from the rather low inter-series correlation between the  $\delta^{13}\text{C}_{\text{TRC}}$  time series, the two conifer species show only minor similarities in their respective climate–proxy relationships (Figure 6). For junipers, the correlations with climate station data reveal mostly weak statistical relationships and therefore a surprisingly weak storage of environmental signals in the  $\delta^{13}\text{C}_{\text{TRC}}$  (Figure 6A). Highly significant positive correlations with climate parameters and juniper  $\delta^{13}\text{C}_{\text{TRC}}$ -variations can only be obtained for different temperature variables during spring season ( $T_{\text{min}}$ ;  $r_{\text{MAM}} = 0.36$ ,  $p < 0.01$ ), and the hydrological year (mean Temperature tmp:  $r_{\text{HydY}} = 0.35$ ,  $p < 0.01$ ). It is apparent that all displayed correlations stay on much lower significance levels than the  $\delta^{18}\text{O}_{\text{TRC}}$ –juniper relationships.

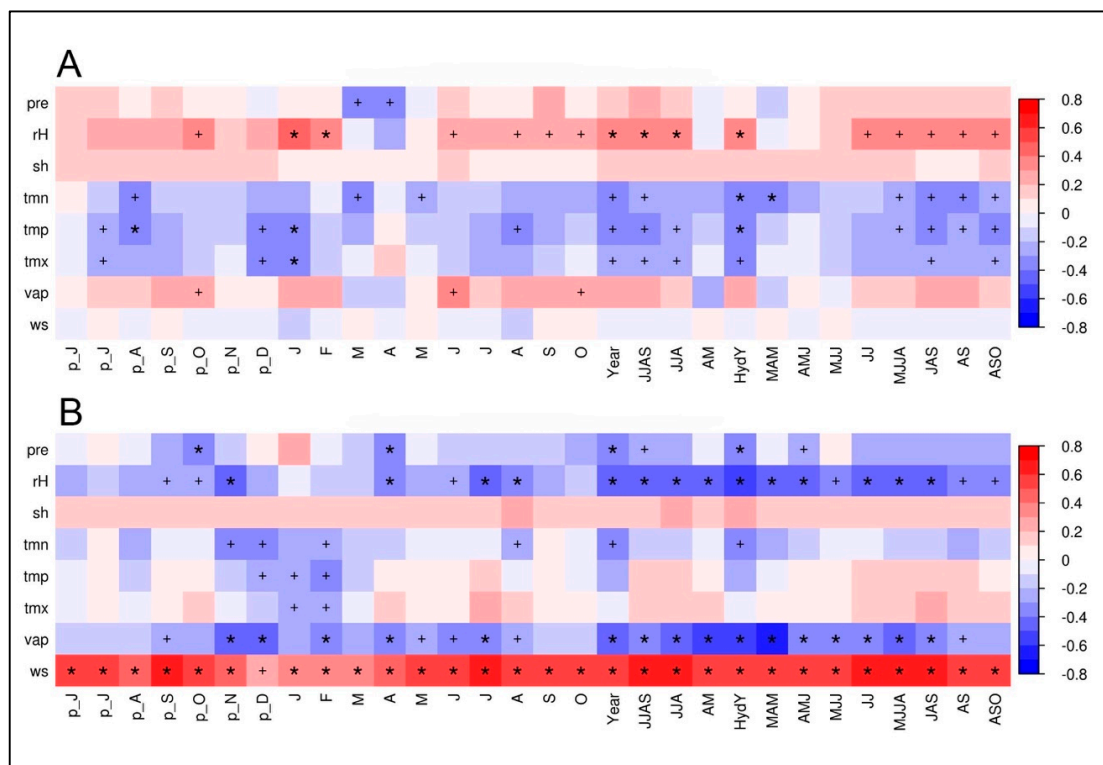


**Figure 6.** Climate–proxy relationships between  $\delta^{13}\text{C}_{\text{TRC}}$  of juniper trees (A) and spruce trees (B) against different monthly and seasonal means of climate parameters (pre, precipitation; rH, relative humidity; sh, sunshine hours; tmn, minimum temperature; tmp, mean temperature; tmx, maximum temperature; vap, vapor pressure deficit; ws, wind speed) from the Qamdo climate station for the period 1954–2007 ( $n = 54$ ). “p” shows relationships to the previous years’ monthly means. Red/blue color indicates a positive/negative correlation coefficient ( $r$ ). The respective level of significance is indicated by a plus sign ( $p < 0.05$ ) or an asterisk ( $p < 0.01$ ).

Figure 6B reveals the correlations between  $\delta^{13}\text{C}_{\text{TRC}}$  values of spruce trees and the climate station in Qamdo. Interestingly, the results are in parts opposite to the correlations for the juniper trees. Especially the change of the sign in the correlation, e.g., for hydroclimate variables such as relative humidity and precipitation, is remarkable. This justifies and confirms that, in the case of  $\delta^{13}\text{C}_{\text{TRC}}$ , the use of a cross-species mean for evaluating proxy–isotope relationships is not appropriate. Highest positive correlations were obtained for wind speed throughout the year, indicating the strong influence of wind on transpiration and gas exchange on leaf level. Significantly negative relationships are apparent for vapor pressure during the hydrological year (November to October) and spring ( $r_{\text{HydY}} = -0.54, p < 0.01$ ;  $r_{\text{MAM}} = -0.58, p < 0.01$ ), and for relative humidity during the hydrological year and the vegetation period ( $r_{\text{HydY}} = -0.53, p < 0.01$ ;  $r_{\text{MJJA}} = -0.50, p < 0.01$ ). It can be concluded that only the spruce  $\delta^{13}\text{C}_{\text{TRC}}$  time series at our study site fulfills the preconditions to reconstruct past environmental history and variability.

As for the  $\delta^{18}\text{O}_{\text{TRC}}$ , we tested climate– $\delta^{13}\text{C}_{\text{TRC}}$  relationships with the CRU TS 4.02 dataset for the period 1901–2007 (Figure S2). Interestingly, correlation coefficients as well as the respective significance levels for juniper are more stable throughout the year than for spruce. This agrees with the results obtained by the analyses with  $\delta^{18}\text{O}_{\text{TRC}}$  (cf. Section 3.3), however, with considerably lower correlation coefficients. For juniper  $\delta^{13}\text{C}_{\text{TRC}}$ , highest correlations are manifested with different temperature variables and potential evaporation (Figure S2A). Highly significant positive correlations of spruce  $\delta^{13}\text{C}_{\text{TRC}}$  occur with diurnal temperature range (dtr), and negative correlations with minimum temperatures (tmn) (Figure S1B).

### 3.5. Implications of Species-Specific Proxy–Climate Responses of Multi-Centennial Isotope Series

Within the subalpine setting and design of our study, across-species  $\delta^{18}\text{O}_{\text{TRC}}$  variations show a very uniform picture in their individual relationships to the tested environmental parameters. The derived climate–proxy correlations clearly indicate that, despite minor differences in exposure and altitude, the same climate and environmental signals are stored in the individual  $\delta^{18}\text{O}_{\text{TRC}}$  variations. The investigated species are regardless of the used climate dataset (climate station or CRU 4.02 dataset) most sensitive to humidity related climate parameters during the vegetation period (May to August), clearly underlining a common external forcing. Among those, relative humidity, precipitation, and maximum temperature have the highest impact. These relationships can be directly linked to the influence of the Asian summer monsoon system, which leads via high amounts of precipitation during the vegetation period season to a relative depletion of  $\delta^{18}\text{O}$  in precipitation (=amount effect) [41]. As a result, negative relationships of  $\delta^{18}\text{O}_{\text{TRC}}$  with hydroclimate parameters such as rH and precipitation occur and are in accordance with plant-physiological models [42,43]. Our findings are corroborated through similar results from numerous studies from the TP and the surrounding areas [10–17,27]. This underlines the straightforward and reasonable fingerprints of summer monsoon signals in  $\delta^{18}\text{O}_{\text{TRC}}$  time-series from the summer monsoon-influenced area.

Minor tree-specific differences are apparent in the absolute values of the derived correlation coefficients, where spruce trees in general show higher values. However, the displayed correlation patterns are very similar in terms of seasonality and signs. The higher sensitivities of spruce trees point to a higher general climate sensitivity compared to the long-living junipers. Since it is not possible to carry out separate analyses of earlywood (EW) and latewood (LW) due to narrow annual rings in junipers with only few rows of latewood, it remains open whether varying climate sensitivities of EW and LW are responsible for the lower signal strength in juniper. An indication of such different sensitivities was found for instance in other studies and species, e.g., from southwestern and southeastern China [23,25]. It has to be noted, however, that these studies are based on significantly shorter time periods of only few years to decades, and use species with significantly wider annual rings compared to ours (*Abies* and *Picea*).

A striking result of our study is that both tree species indicate over the full common period of approximately 400 years a very high conformity in different frequency ranges. Hereby, a very high agreement can be found for single positive and negative extreme years as well as for lower frequency ranges, underlining the uniform response to a common forcing. This is confirmed by the climate–proxy relationship of the cross-species mean isotope chronology compared to the individual species chronologies. When analyzing the climate–isotope response of the average value, species-specific correlations are retained highly significant in both, their response and temporal linkage (individual months and seasons). Consequently, the spatial representativity of both oxygen time series should be expectedly similar. In fact, the analysis of spatial correlations with the three different  $\delta^{18}\text{O}_{\text{TRC}}$  datasets using the KNMI climate explorer (<https://climexp.knmi.nl>) allows this relationship to be further quantified (Figure 7). The discussed higher sensitivity of spruce trees compared to junipers also results in consistently higher spatial correlations with different humidity and drought parameters. These are insofar as from a theoretical perspective of isotope fractionation and fixation reasonable, since they display an often reported negative (MJJJ precipitation and MJJJ scPDSI) or positive relationship (increased evaporation during the summer season via  $T_{\text{Max}}$ ) mainly caused by a precipitation amount or temperature effect during the summer monsoon season. Interestingly, Figure 7 displays that the high spatial correlations remain stable with the calculation of a species' mean and thus validates a general high common sensitivity to hydroclimate variables and large spatial representativity of multi-century oxygen isotope time-series across species. This uniform behavior across species further underlines the suitability and applicability of annually resolved, tree-ring based stable oxygen isotope time series to serve as an independent dating control for other archives (e.g., ice cores), as suggested in [44].

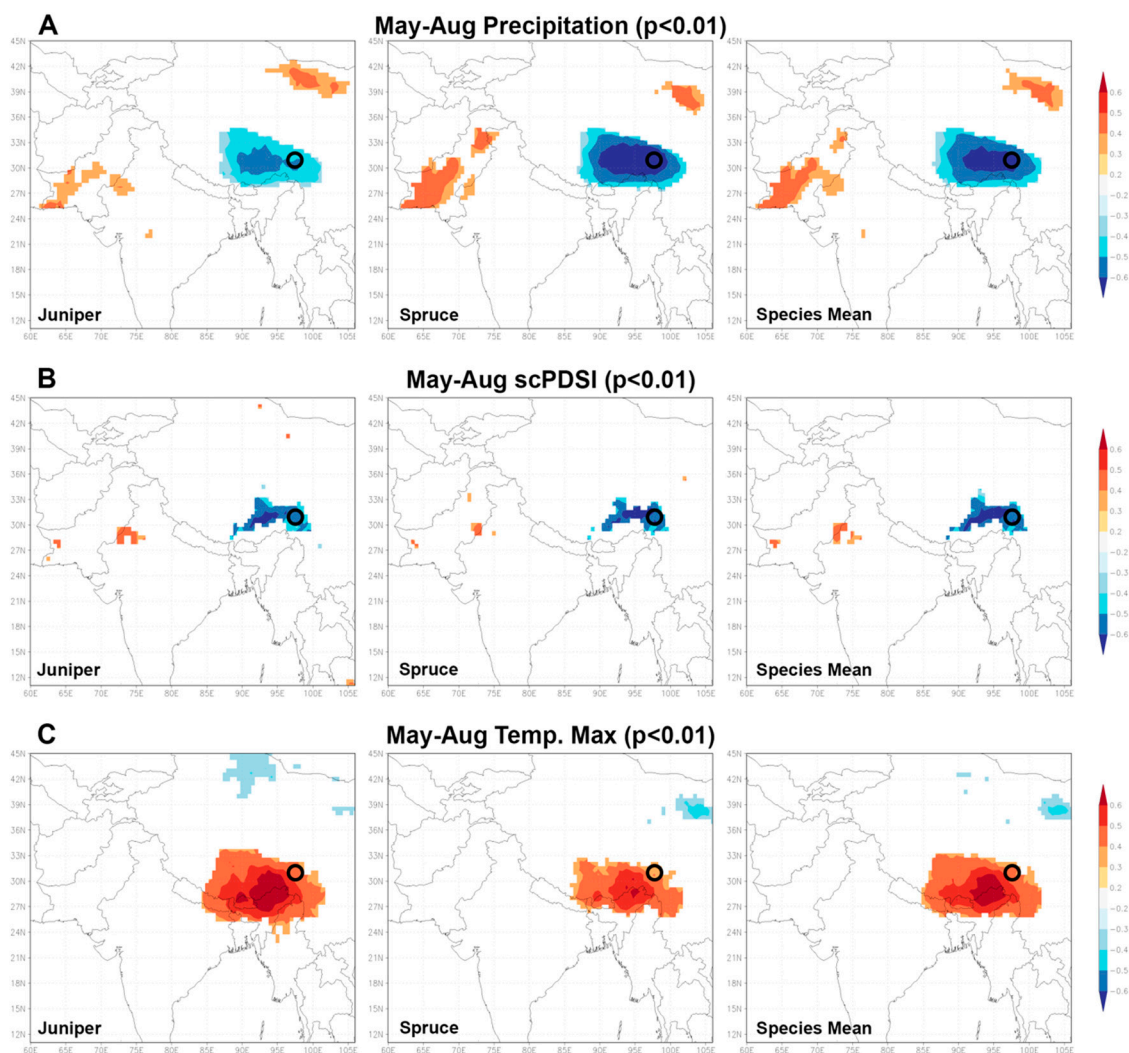


**Figure 7.** Spatial correlations ( $p < 0.01$ ) of  $\delta^{18}\text{O}$  variations in juniper, spruce and the species' mean (vertically arranged) with climate variables using the Climate Explorer. (A–C) Selected climate variables for the individual species (juniper and spruce) and the calculated  $\delta^{18}\text{O}$  mean of our study site for the summer monsoon season (May to August).

It is striking that, in contrast to the investigated oxygen isotope series, the derived  $\delta^{13}\text{C}_{\text{TRC}}$  series reveal a low common signal across species combined with a missing uniform response to the tested environmental parameters. This confirms results of previous studies on  $\delta^{13}\text{C}_{\text{TRC}}$  from China, where no common cross-regional proxy signal has been found [25,44–48]. Instead, these studies suggest that the respective  $\delta^{13}\text{C}_{\text{TRC}}$  series rather display more site-related ecophysiological responses on a changing environment. This can be underlined by the variety of interpretations according to which the respective  $\delta^{13}\text{C}_{\text{TRC}}$  series serves as a proxy for changes in the plant-internal water-use strategy [25,28], as a proxy for temperature during the vegetation period [45], and for summer temperatures [46]. Only few studies indicate a dependency of  $\delta^{13}\text{C}_{\text{TRC}}$  variations on moisture conditions (including precipitation and rH) [47,48]. This is probably connected to a generally drier setting at the investigation site and therefore a higher drought limitation at these sites compared to our location.

Although we can infer for both studied species at our study site similar macro- and mesoclimatic conditions and soil characteristics, differing physiological factors and processes seem to overprint or bias the detection of dominant environmental signals in our tree-ring  $\delta^{13}\text{C}$ . As mentioned in [33,38–40],  $^{13}\text{C}$  variations in tree-rings are on the one hand controlled by external environmental factors that regulate the uptake of atmospheric  $\text{CO}_2$  via the stomata of the leaves. Stomatal conductivity is in

turn mainly determined by factors such as rH, temperature, moisture and wind. On the other hand, the carbon isotopes of CO<sub>2</sub> are subject to a fractionation at the enzyme RUBISCO dependent on the respective CO<sub>2</sub> concentration within the leaves. This, e.g., results in a discrimination in favor to the lighter <sup>12</sup>C and against the heavier <sup>13</sup>C isotopes during photosynthesis. Therefore, sensitivities and responses of the individual  $\delta^{13}\text{C}_{\text{TRC}}$  to humidity parameters like rH and maximum temperature would be expectable. However, this is not straightforward displayed in our results. Instead, results of climate–isotope correlations with relative humidity indicate an indistinct, species-specific response during the vegetation period (positive for junipers, negative for spruce).

The displayed negative results for correlations between  $\delta^{13}\text{C}_{\text{TRC}}$  of spruce and rH are in so far expectable and reasonable since a higher rH during the vegetation period linked to more open stomata leads to a depletion in  $\delta^{13}\text{C}_{\text{TRC}}$ . This relationship stays stable for different seasonal means and single months during the vegetation period. Therefore, a seasonally higher moisture availability during the summer monsoon season apparently does not seem to be decisive for the regulations of the stomata. Presumably, moisture is not the main limiting factor for spruce during the summer monsoon season, although monsoonally triggered higher temperatures and humidity are then predominant. A higher moisture availability during the summer season leads to a further increase in the discrimination against <sup>13</sup>C. For juniper, the explanation of the positive relationship between  $\delta^{13}\text{C}_{\text{TRC}}$  and rH remains at this point challenging. As mentioned, conditions with higher humidity during the summer monsoon season would expectably be associated to more favorable conditions resulting in wider opened stomata. This will in turn result in lower  $\delta^{13}\text{C}_{\text{TRC}}$  values. Thus, a negative correlation between  $\delta^{13}\text{C}_{\text{TRC}}$  and the relative humidity would be expected as consequently displayed by the spruce  $\delta^{13}\text{C}_{\text{TRC}}$ . Since correlations with a more radiation related parameter such as sunshine hours for the junipers do not display any significant result, possible short-range differences in humidity between both tree stands can be excluded as the reason for this. At this stage, explanations for such differences between species cannot be evaluated without knowledge of possibly underlying and possibly biasing plant-internal factors.

It remains striking that the climate  $\delta^{13}\text{C}_{\text{TRC}}$  relationships are compared to the results derived from the  $\delta^{18}\text{O}_{\text{TRC}}$  significantly lower and somehow inconsistent in terms of a uniform (site and species) signal and representativity. In addition, the underlying long-term trend especially apparent for the spruce trees clearly hampers the decoding of climate signals in our  $\delta^{13}\text{C}_{\text{TRC}}$  series. To evaluate the influence of low-frequency variations on the different species and isotopes, high-pass filtered versions of all time-series were correlated against the climate station data. In the  $\delta^{18}\text{O}_{\text{TRC}}$  series, the removal of the low-frequency variations which can be visualized through wavelets (Figure S3) results in slightly less strong, but still consistent correlation patterns. For the  $\delta^{13}\text{C}_{\text{TRC}}$  series, the high-pass filtering removes the significance in the juniper–climate relationships almost completely. Contrasting, the correlations of the spruce  $\delta^{13}\text{C}_{\text{TRC}}$  series with climate are enhanced in the positive (temperature) as well as negative (precipitation, rH, and vapor pressure) directions. Although correlations vary over time, this suggests that species-specific correlations with climate data since the 1960s are highly dependent on the chosen trend correction method. This is additionally corroborated by the difference displayed in moving correlations between the raw  $\delta^{13}\text{C}_{\text{TRC}}$  series and the CO<sub>2</sub>-corrected  $\delta^{13}\text{C}_{\text{TRC}}$  series (Figure S4). Such an influence of the chosen trend correction is in line with the results of [45].

### 3.6. Long-Term Trends in Carbon Isotope Ratios and their Implications for Recording Climate Signals

As displayed in Figure 4, even the corrected  $\delta^{13}\text{C}_{\text{TRC}}$  time series do not indicate a uniform signal between species. In contrast to  $\delta^{18}\text{O}_{\text{TRC}}$ , the  $\delta^{13}\text{C}_{\text{TRC}}$  series reveal for both species a highly individual year-to-year variability as well as negative long-term trends. In addition, since 1900, a significantly more negative trend in spruce  $\delta^{13}\text{C}_{\text{TRC}}$  values as compared to the juniper values is evident. By taking into account approximately comparable site conditions for both studied species, only certain internal physiological drivers can probably lead to the stronger depletion of the heavier <sup>13</sup>C isotopes in the spruce trees. Thus, we assume that species-specific ecophysiological responses

to increasing atmospheric CO<sub>2</sub> or to increasing temperatures cause differences in the uptake of heavier <sup>13</sup>C in the tree-rings. The impact of this changing external forcing and the resulting different response of the two tree species become even more impressive when considering the δ<sup>13</sup>C<sub>TRC</sub> in a multi-centennial perspective.

Global and regional studies show that trees tend to respond to an increase in atmospheric CO<sub>2</sub> through various ecophysiological adaptations, such as modulations in the response of photosynthesis, stomatal conductance, or a response in the water-use efficiency (iWUE) [49–54]. It is likely that the substantial disparities and trends in our δ<sup>13</sup>C<sub>TRC</sub> series display species-specific ecophysiological reactions to a rising atmospheric CO<sub>2</sub> concentration and/or to a substantial altitude-dependent increase in temperature on the TP [55,56]. Recently, it is reported that even within a sampling site such reactions can be species-specific [57]. Consequently, such plant-internal adaptations will in turn lead to a blurred picture of climatic signals stored in the respective δ<sup>13</sup>C<sub>TRC</sub> values. The apparent negative δ<sup>13</sup>C<sub>TRC</sub> after correction for atmospheric CO<sub>2</sub> change can be therefore one reason for the weak correlations of δ<sup>13</sup>C<sub>TRC</sub> with climate parameters. In addition, the choice of the suitable correction factor can have an influence that should not be underestimated, as reported in [43]. Probably our carbon isotope time-series indicate an individual response of the investigated tree species towards the changing CO<sub>2</sub> concentrations rather than recording an environmental signal.

Figure 8 shows the iWUE of the two investigated tree species for the period 1900–2007. With respect to the reported environmental change in terms of a general warming trend since the 1950s, we additionally split the investigation period into two individual segments with a threshold in 1955. It is apparent that the displayed individual iWUEs differ in their absolute amounts as well as in their long-term trends for the full period between the species. This points to different species-specific physiological strategies and adaptations either with regard to changes in climate and/or changes in the atmospheric CO<sub>2</sub> concentration. Whereas the iWUE of juniper trees is characterized by a more or less stable phase throughout the early period (−2% for the period 1900–1954), a steady and strong increase in the iWUE is apparent since the 1960s (+20%), reaching a maximum in 2005. With regard to the full period from 1900 to 2007, the relative increase in iWUE for juniper is 17%. In comparison, spruce tree iWUE is characterized by a slight increase (+1%) during 1900–1954. Similar to the juniper trees, spruce trees show a remarkably positive trend towards a higher iWUE for the recent six decades and therefore an adaptation for reducing water loss through transpiration. However, the absolute increase in iWUE of spruce since 1955 is markedly lower (+14%) and also evolves in its long-term rate during 1900–2007 generally slower than in juniper (+12%). *Juniperus* as a more drought tolerant species can probably better respond and react to the ongoing environmental changes with rising temperatures and lower humidity with a faster acceleration within their respective iWUE. On the other hand, more favorable microclimatic conditions with higher humidity at the spruce stands might help this species to better cope with the increase in temperature. The different trends and responses in iWUE indicate that plant physiological adaptations to changing external environmental parameters can be detected for both tree species. These plant physiological adaptations aggravate a more straightforward interpretation of our climate–proxy relationships. A necessary deciphering need in turn further analyses on the responsible plant-internal drivers. The future use of our δ<sup>13</sup>C<sub>TRC</sub> time series for climate reconstruction appears at this stage therefore challenging. Although admittedly reflecting an initial stage, our results on the iWUE are in good accordance to existing studies from the Tibetan Plateau dealing with *Pinus* and *Abies* species, where similar positive trends in iWUE were reported for the last decades [28,58]. In addition, on a global scale, such responses can be observed in various tree species, e.g., from the tropics [59,60] or more temperate zones [53,61–66].



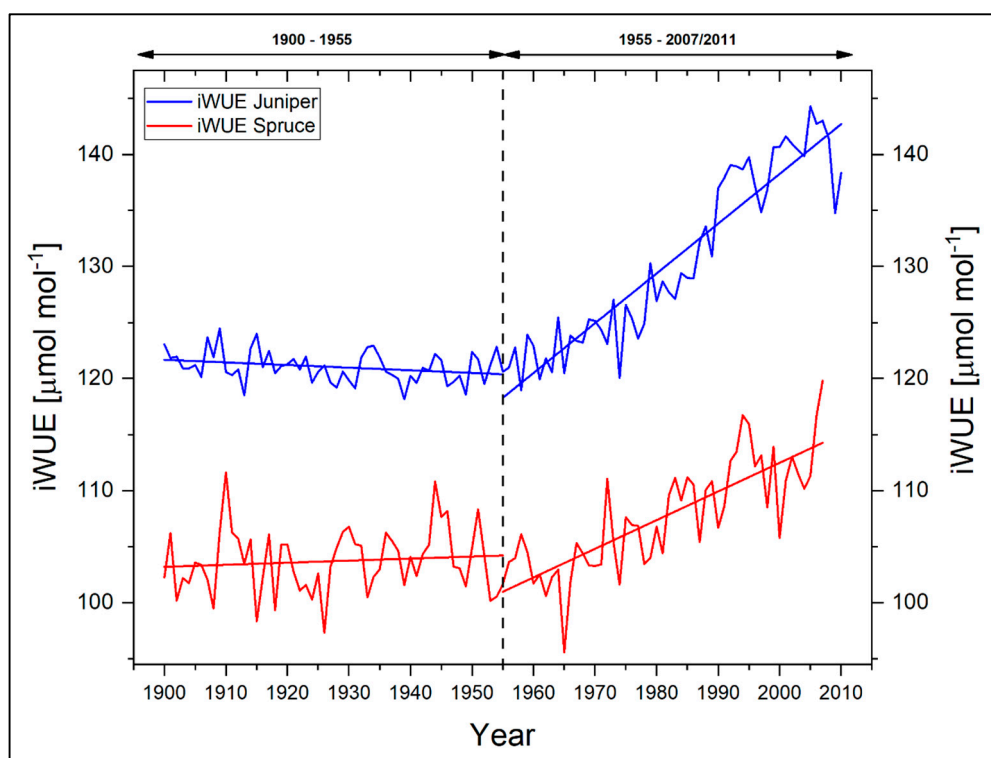


**Figure 8.** Intrinsic water-use efficiencies for *Juniperus tibetica* and *Picea balfouriana* at Qamdo. Dashed line indicates dividing line between the investigation periods, while old lines represent the individual linear trends of both species for the periods 1900–1954 and 1955–2007, respectively.

We are aware that substantial ecophysiological investigations on and interpretations of iWUE need more knowledge about the corresponding changes in controlling plant physiological and environmental factors (e.g.,  $c_i$ ,  $c_a$ , and the carbon isotope discrimination  $\Delta$ ). Since this study mainly targeted a first estimation of the usability and the included potentials and limitations of a dual isotope and dual species approach at a single site, we focused on a first qualitative description of ecophysiological findings. Therefore, the identification and quantification of the proportion or the combination of, e.g., temperature rise and  $\text{CO}_2$  concentration, on the two tree species clearly exceeds the scope of the presented manuscript. More complex and further comprehensive ecophysiological analyses of the obtained results will be subjects of an upcoming study.

#### 4. Conclusions

This study represents the first substantial comparison of annually resolved, multi-centennial tree-ring  $\delta^{13}\text{C}$  and  $\delta^{18}\text{O}$  isotope time series from a high mountain site at the southeastern Tibetan Plateau. Although the external forcings and general site characteristics can be regarded as highly comparable, a thorough evaluation on responsible environmental factors causing the respective  $\delta^{13}\text{C}_{\text{TRC}}$  and  $\delta^{18}\text{O}_{\text{TRC}}$  variations in the tree species revealed in part substantial differences.

The displayed  $\delta^{18}\text{O}_{\text{TRC}}$  variations of juniper and spruce trees show a congruent response to the analysed climate parameters, indicating a uniform response across species to a common forcing. As best results were obtained for various hydroclimatic parameters during the vegetation period, notably a summer monsoon signal was herein recorded. By combining and averaging the  $\delta^{18}\text{O}_{\text{TRC}}$  time series of our investigated species, existing highly significant proxy–climate relationships on selected hydroclimatic variables could be in most cases retained. Microclimatic influences and/or species-specific differences in the individual tree species are presumably reduced in favor to a more representative and common site signal. Thus, when analyzing  $\delta^{18}\text{O}$  in tree-rings, the expressiveness of  $\delta^{18}\text{O}_{\text{TRC}}$ -time series can be enhanced by studying two tree species at one location.

In contrast, only weak relationships occur between the  $\delta^{13}\text{C}_{\text{TRC}}$  series and tested environmental parameters. This is all the more astonishing as the locations of both tree stands are close to each other. Consequently, mainly plant-internal strategies and species-specific effects or adaptations are biasing the recording of climate signals. In combination with a—still strongly preserved—long-term trend after atmospheric  $\text{CO}_2$  trend correction in spruce, several questions remain open for an unambiguous interpretation of the  $\delta^{13}\text{C}_{\text{TRC}}$  variations. Both studied species apparently reflect an individual response to environmental change. Juniper trees situated at higher elevations and southerly exposed react more sensitively with regards to the increasing irradiation and decrease in cloud cover and rH. This is for example evident from the changes in the iWUE. For spruce trees, the microclimatic advantage of a comparably higher humidity may be favorable, resulting in a delayed, lowered and lagged increase in iWUE. A verification of this assumption, however, requires a separate investigation, which should also include studies on seasonal isotope variations and coupled plant-internal effects.

Nevertheless, such species-specific investigations on similar settings might help to predict the influence and impact of future climate change on the adaptation ability of dominant tree species in the area of the treeline ecotone on the Tibetan plateau. For a quantification of such plant-internal responses, future studies should evaluate the complex interaction on the impact of a probable  $\text{CO}_2$ -fertilization effect on iWUE, a general rise in temperature on the photosynthetic rate, and the interplay of growth and iWUE.

**Supplementary Materials:** The following are available online at <http://www.mdpi.com/2076-3263/9/4/151/s1>, Figure S1. Climate–proxy correlation of: juniper  $\delta^{18}\text{O}_{\text{TRC}}$  (A); spruce  $\delta^{18}\text{O}_{\text{TRC}}$  (B); and the site-internal  $\delta^{18}\text{O}_{\text{TRC}}$  mean (C) against monthly and seasonal means of different gridded climate parameters from the CRU TS4.01 dataset for the period 1954–2007 (cld, cloud cover; dtr, diurnal temperature range; frs, number of frost days; pet, potential evapotranspiration; tmn, minimum temperature; tmp, mean temperature; tmx, maximum temperature; wet, wet days frequency). “p” shows relationships to the previous years’ monthly means. Red/blue colour indicate positive/negative correlation coefficients (r). The respective level of significance is indicated by a plus sign ( $p < 0.05$ ) or an asterisk ( $p < 0.01$ ); Figure S2. Climate–proxy correlation between juniper  $\delta^{13}\text{C}_{\text{TRC}}$  (A) and spruce  $\delta^{13}\text{C}_{\text{TRC}}$  (B) against different monthly and seasonal means of gridded climate parameters from the CRU TS4.01 dataset for the period 1954–2007 (cld, cloud cover; dtr, diurnal temperature range; frs, number of frost days; pet, potential evapotranspiration; tmn, minimum temperature; tmp, mean temperature; tmx, maximum temperature; wet, wet days frequency). “p” shows relationships to the previous years’ monthly means. Red/blue colors indicate positive/negative correlation coefficients (r). The respective level of significance is indicated by a plus sign ( $p < 0.05$ ) or an asterisk ( $p < 0.01$ ); Figure S3. Wavelet analyses (Morlet) for both isotopes and species during the common period (1685–2007); (left) original values; and (right) high-pass filtered version. Periods of significant periodicities are framed by white lines; Figure S4. Moving correlations (50-year windows) between the raw  $\delta^{13}\text{C}$  series of spruce and juniper (in violet) and the  $\text{CO}_2$ -corrected  $\delta^{13}\text{C}$  series of the investigated two tree species (in orange).

**Author Contributions:** Conceptualization, J.G.; analysis and visualization, J.G., W.J.-H.M., and P.H.; methodology, writing and original draft preparation, all authors; and funding acquisition, J.G., G.H.S., and A.B.

**Funding:** This research was partly funded by the German Research Foundation DFG, grant number BR1895/21-1.

**Acknowledgments:** The authors are grateful to the laboratory staffs from the German Research Centre of Jülich and of the Institute of Geography of the Friedrich-Alexander-University of Erlangen-Nürnberg for their assistances during the analytical analyses. We thank the three reviewers for their substantial help to improve the manuscript and R. Huang for sharing his data. The presented datasets are available after acceptance throughout the PANGAEA online platform ([www.pangaea.de](http://www.pangaea.de)).

**Conflicts of Interest:** The authors declare no conflict of interest. The funders had no role in the design of the study; in the collection, analyses, or interpretation of data; in the writing of the manuscript, or in the decision to publish the results.

## References

1. Yao, T.; Thompson, L.; Yang, W.; Yu, W.; Gao, Y.; Guo, X.; Yang, X.; Duan, K.; Zhao, H.; Xu, B.; et al. Different glacier status with atmospheric circulations in Tibetan plateau and surroundings. *Nat. Clim. Chang.* **2012**, *2*, 663–667. [[CrossRef](#)]
2. Immerzeel, W.; van Beek, L.; Bierkens, M. Climate Change will affect the Asia Water Towers. *Science* **2010**, *328*, 1382–1385. [[CrossRef](#)] [[PubMed](#)]

3. Royden, L.H.; Burchfiel, B.C.; van der Hilst, R.R. The geological evolution of the Tibetan plateau. *Science* **2008**, *321*, 1054–1058. [[CrossRef](#)]
4. Böhner, J. General climatic controls and topoclimatic variations in Central and High Asia. *Boreas* **2006**, *35*, 279–295. [[CrossRef](#)]
5. Yang, K.; Wu, H.; Qin, J.; Lin, C.; Tang, W.; Chen, Y. Recent climate changes over the Tibetan plateau and their impacts on energy and water cycle: A review. *Glob. Planet. Chang.* **2014**, *112*, 79–91. [[CrossRef](#)]
6. Yang, K.; Ye, B.; Zhou, D.; Wu, B.; Foken, T.; Qin, J.; Zhou, Z. Response of the hydrological cycle to recent climate changes in the Tibetan plateau. *Clim. Chang.* **2011**, *109*, 517–534. [[CrossRef](#)]
7. Cheng, G.; Wu, T. Responses of permafrost to climate change and their environmental significance, Qinghai-Tibet plateau. *J. Geophys. Res.* **2007**, *112*, F02S03. [[CrossRef](#)]
8. Kang, S.; Xu, Y.; You, Q.; Flügel, W.A.; Pepin, N.; Yao, T. Review of climate and cryospheric change in the Tibetan plateau. *Environ. Res. Lett.* **2010**, *5*, 01510. [[CrossRef](#)]
9. Yang, B.; He, M.; Shishov, V.; Tychkov, I.; Vaganov, E.; Rossi, S.; Ljungqvist, F.C.; Bräuning, A.; Griesinger, J. New perspective on spring vegetation phenology and global climate change based on Tibetan Plateau tree-ring data. *Proc. Natl. Acad. Sci. USA* **2017**, *114*, 6966–6971. [[CrossRef](#)] [[PubMed](#)]
10. Shi, C.; Daux, V.; Zhang, Q.-B.; Risi, C.; Hou, S.-G.; Stievenard, M.; Pierre, M.; Li, Z.; Masson-Delmotte, V. Reconstruction of southeast Tibetan plateau summer climate using tree ring  $^{18}\text{O}$ : Moisture variability over the past two centuries. *Clim. Past* **2012**, *8*, 205–213. [[CrossRef](#)]
11. Griesinger, J.; Bräuning, A.; Helle, G.; Thomas, A.; Schleser, G.H. Late Holocene Asian summer monsoon variability reflected by  $\delta^{18}\text{O}$  in tree-rings from Tibetan junipers. *Geophys. Res. Lett.* **2011**, *38*, L03701. [[CrossRef](#)]
12. Griesinger, J.; Bräuning, A.; Helle, G.; Hochreuther, P.; Schleser, G.H. Late Holocene relative humidity history on the southeastern Tibetan plateau inferred from a tree-ring  $\delta^{18}\text{O}$  record: Recent decrease and conditions during the last 1500 years. *Quat. Int.* **2017**, *430*, 52–59. [[CrossRef](#)]
13. Wernicke, J.; Hochreuther, P.; Griesinger, J.; Zhu, H.; Wang, L.; Bräuning, A. Multi-century humidity reconstructions from the southeastern Tibetan Plateau inferred from tree-ring  $\delta^{18}\text{O}$ . *Glob. Planet. Chang.* **2016**, *149*. [[CrossRef](#)]
14. Wernicke, J.; Griesinger, J.; Hochreuther, P.; Bräuning, A. Variability of summer humidity during the past 800 years on the eastern Tibetan Plateau inferred from  $\delta^{18}\text{O}$  of tree-ring cellulose. *Clim. Past* **2015**, *11*, 327–337. [[CrossRef](#)]
15. Hochreuther, P.; Wernicke, J.; Griesinger, J.; Mölg, T.; Zhu, H.; Wang, L.; Bräuning, A. Influence of the Indian Ocean Dipole on tree-ring  $\delta^{18}\text{O}$  of monsoonal Southeast Tibet. *Clim. Chang.* **2016**, *137*, 217–230. [[CrossRef](#)]
16. Xu, G.; Liu, X.; Trouet, V.; Treydte, K.; Wu, G.; Chen, T.; Sun, W.; An, W.; Wang, W.; Zeng, X.; et al. Regional shifts (1710–2019) in East Central Asia and linkages with atmospheric circulation recorded in tree-ring  $\delta^{18}\text{O}$ . *Clim. Dyn.* **2018**. [[CrossRef](#)]
17. Liu, X.; Xu, G.; Griesinger, J.; An, W.; Wang, W.; Zeng, X.; Wu, G.; Qin, D. A shift in cloud cover over the southeastern Tibetan plateau since 1600, evidence from regional tree-ring  $^{18}\text{O}$  and its linkages to tropical oceans. *Quat. Sci. Rev.* **2014**, *88*, 55–68. [[CrossRef](#)]
18. McCarroll, D.; Gagen, M.H.; Loader, N.J.; Robertson, I.; Anchukaitis, K.J.; Los, S.; Young, G.H.F.; Jalkanen, R.; Kirchhefer, A.; Waterhouse, J.S. Correction of tree ring stable carbon isotope chronologies for changes in the carbon dioxide content of the atmosphere. *Geochim. Cosmochim. Acta* **2009**, *73*, 1539–1547. [[CrossRef](#)]
19. Loader, N.J.; McCarroll, D.; Gagen, M.; Robertson, I.; Jalkanen, R. Extracting climatic informations from stable isotopes in tree rings. In *Stable Isotopes as Indicators of Ecological Change*; Dawson, T.E., Siegwolf, R.T.W., Eds.; Elsevier: Amsterdam, The Netherlands, 2007; pp. 27–48.
20. Xu, G.; Liu, X.; Qin, D.; Chen, T.; Sun, W.; An, W.; Wang, W.; Wu, G.; Zeng, X.; Ren, J. Drought history inferred from tree ring  $^{13}\text{C}$  and  $^{18}\text{O}$  in the central Tianshan Mountains of China and linkage with the North Atlantic Oscillation. *Theor. Appl. Climatol.* **2014**, *116*, 385–401. [[CrossRef](#)]
21. Xu, G.; Liu, X.; Belmecheri, S.; Chen, T.; Wu, G.; Wang, B.; Zeng, X.; Wang, W. Disentangling Contributions of  $\text{CO}_2$  Concentration and Climate to Changes in intrinsic water-use efficiency in the arid boreal forest in China's Altay Mountains. *Forests* **2018**, *9*, 642. [[CrossRef](#)]
22. Xu, G.; Liu, X.; Sun, W.; Chen, T.; Zhang, X.; Zeng, X.; Wu, G.; Wang, W.; Qin, D. Application and verification of simultaneous determination of cellulose  $\delta^{13}\text{C}$  and  $\delta^{18}\text{O}$  in *Picea shrenkiana* tree rings from northwestern China using the high-temperature pyrolysis method. *J. Arid Land* **2018**, *10*, 864–876. [[CrossRef](#)]

23. An, W.; Liu, X.; Leavitt, S.W.; Ren, J.; Sun, W.; Wang, W.; Wang, Y.; Xu, G.; Chen, T.; Qin, D. Specific climatic signals recorded in earlywood and latewood  $^{18}\text{O}$  of tree rings in southwestern China. *Tellus B* **2012**, *64*, 18703. [[CrossRef](#)]
24. Hartl-Meier, C.; Zang, C.; Büntgen, U.; Esper, J.; Rothe, A.; Göttelein, A.; Dirnböck, T.; Treydte, K. Uniform climate sensitivity in tree-ring stable isotopes across species and sites in a mid-latitude temperate forest. *Tree Physiol.* **2014**, *35*, 4–15. [[CrossRef](#)] [[PubMed](#)]
25. Fu, P.; Griesinger, J.; Gebrekirstos, A.; Fan, Z.-X.; Bräuning, A. Earlywood and Latewood Stable Carbon and Oxygen Isotope Variations in Two Pine Species in Southwestern China during the Recent Decades. *Front. Plant Sci.* **2017**, *7*, 2050. [[CrossRef](#)] [[PubMed](#)]
26. Zeng, X.; Liu, X.; Treydte, K.; Evans, M.N.; Wang, W.; An, W.; Sun, W.; Xu, G.; Wu, G.; Zhang, X. Climate signals in tree-ring  $\delta^{18}\text{O}$  and  $\delta^{13}\text{C}$  from southeastern Tibet: Insights from observations and forward modelling of intra- to interdecadal variability. *New Phytol.* **2017**, *216*, 1104–1118. [[CrossRef](#)] [[PubMed](#)]
27. He, M.; Yang, B.; Bräuning, A.; Rossi, S.; Ljungqvist, F.C.; Shishov, V.; Griesinger, J.; Wang, J.; Liu, J.; Qin, C. Recent advances in dendroclimatology in China. *Earth-Sci. Rev.* **2019**. [[CrossRef](#)]
28. Huang, R.; Zhu, H.; Liu, X.; Liang, E.; Griesinger, J.; Wu, G.; Li, X.; Bräuning, A. Does increasing intrinsic water use efficiency (iWUE) stimulate tree growth at natural timberline on the southeastern Tibetan plateau? *Glob. Planet. Chang.* **2017**, *148*, 217–226. [[CrossRef](#)]
29. Bräuning, A. Climate history of the Tibetan plateau during the last 1000 years derived from a network of Juniper chronologies. *Dendrochronologia* **2001**, *19*, 127–137.
30. Zhu, H.; Shao, X.; Yin, J.; Huang, L. Early summer temperature reconstruction in the eastern Tibetan plateau since AD 1440 using tree-ring width of *Sabina tibetica*. *Theor. Appl. Clim.* **2011**, *106*, 45–53. [[CrossRef](#)]
31. Miehe, G.; Miehe, S.; Vogel, J.; La, D. Highest tree-line in the northern hemisphere found in southern Tibet. *Mt. Res. Dev.* **2007**, *27*, 169–173. [[CrossRef](#)]
32. Leavitt, S. Tree-ring C-H-O isotope variability and sampling. *Sci. Total Environ.* **2010**, *408*, 5244–5253. [[CrossRef](#)]
33. McCarroll, D.; Loader, N.J. Stable isotopes in tree rings. *Quat. Sci. Rev.* **2004**, *23*, 771–801. [[CrossRef](#)]
34. Wieloch, T.; Helle, G.; Heinrich, I.; Voight, M.; Schyma, P. A novel device for batch-wise isolation of a-cellulose from small-amount wholewood samples. *Dendrochronologia* **2011**, *29*, 115–117. [[CrossRef](#)]
35. Laumer, W.; Andreau, L.; Helle, G.; Schleser, G.H.; Wieloch, T.; Wissel, H. A novel approach for the homogenization of cellulose to use micro-amounts for stable isotope analyses. *Rapid Commun. Mass Spectrom.* **2009**, *23*, 1934–1940. [[CrossRef](#)] [[PubMed](#)]
36. Harris, I.; Jones, P.D.; Osborn, T.J.; Lister, D.H. Updated high-resolution grids of monthly climatic observations—The CRU TS 3.10 dataset. *J. Clim.* **2014**, *34*, 623–642. [[CrossRef](#)]
37. R Core Team. A Language and Environment for Statistical Computing. R Foundation for Statistical Computing. 2013. Available online: [www.R-project.org/](http://www.R-project.org/) (accessed on 1 March 2019).
38. MacFarling Meure, C.; Etheridge, D.; Trudinger, C.; Steele, P.; Langenfelds, R.; Van Ommen, T.; Smith, A.; Elkins, J. Law Dome  $\text{CO}_2$ ,  $\text{CH}_4$  and  $\text{N}_2\text{O}$  ice core records extended to 2000 years BP. *Geophys. Res. Lett.* **2006**, *33*, L14810. [[CrossRef](#)]
39. Ehleringer, J.R.; Hall, A.E.; Farquhar, G.D. *Stable Isotopes and Plant Water Relations*; Elsevier: Dordrecht, The Netherlands, 1993.
40. Farquhar, G.D.; O’Leary, M.; Berry, J. On the relationship between carbon isotope discrimination and the intercellular carbon dioxide concentration in leaves. *Funct. Plant Biol.* **1982**, *9*, 121–137. [[CrossRef](#)]
41. Dansgaard, W. Stable isotopes in precipitation. *Tellus* **1964**, *4*, 436–468.
42. Barbour, M. Stable oxygen isotope composition of pant tissue: A review. *Funct. Plant Biol.* **2007**, *34*, 83–94. [[CrossRef](#)]
43. Gessler, A.; Ferrio, J.P.; Hommel, R.; Treydte, K.; Werner, R.A.; Monson, R.K. Stable isotopes in tree rings e toward a mechanistic understanding of isotope fractionation and mixing processes from the leaves to the wood. *Tree Physiol.* **2014**, *34*, 796–818. [[CrossRef](#)] [[PubMed](#)]
44. Huang, R.; Zhu, H.; Liang, E.; Griesinger, J.; Wernicke, J.; Yu, W.; Hochreuther, P.; Risi, C.; Zeng, Y.; Fremme, A.; et al. Temperature signals in tree-ring oxygen isotope series from the northern slope of the Himalaya. *Earth Planet. Sci. Lett.* **2018**, *506*, 455–465. [[CrossRef](#)]

45. Wang, W.; Liu, X.; Shao, X.; Leavitt, S.; Xu, G.; An, W.; Qin, D. A 200 year temperature record from tree ring  $\delta^{13}\text{C}$  at the Qaidam Basin of the Tibetan Plateau after identifying the optimum method to correct for changing atmospheric  $\text{CO}_2$  and  $\delta^{13}\text{C}$ . *J. Geophys. Res. Biogeosci.* **2011**, *116*, G04022. [[CrossRef](#)]
46. Liu, Y.; Wang, Y.; Li, Q.; Song, H.; Linderholm, H.W.; Leavitt, S.W.; Wang, R.; An, Z. Tree-ring stable carbon isotope-based May–July temperature reconstruction over Nanwutai, China, for the past century and its record of 20<sup>th</sup> century warming. *Quat. Sci. Rev.* **2014**, *93*, 67–76. [[CrossRef](#)]
47. Liu, Y.; Ta, W.; Li, Q.; Song, H.; Sun, C.; Cai, Q.; Liu, H.; Wang, L.; Hu, S.; Sun, J.; et al. Tree-ring stable carbon isotope-based April–June relative humidity reconstruction since AD 1648 in Mt. Tianmu, China. *Clim. Dyn.* **2017**, *50*, 1733–1745. [[CrossRef](#)]
48. Liu, Y.; Ma, L.; Leavitt, S.W.; Cai, Q.; Liu, W. A preliminary seasonal precipitation reconstruction from tree-ring stable carbon isotopes at Mt. Helan, China, since AD 1804. *Glob. Planet. Chang.* **2004**, *41*, 229–239. [[CrossRef](#)]
49. Körner, C.; Paulsen, J. A world wide study of high altitude treeline temperatures. *J. Biogeogr.* **2004**, *31*, 713–732. [[CrossRef](#)]
50. Hyvönen, R.; Agren, G.I.; Linder, S.; Persson, T.; Cotrufo, M.F.; Ekblad, A.; Freeman, M.; Grelle, A.; Janssens, I.A.; Jarvis, P.G.; et al. The likely impact of elevated  $\text{CO}_2$ , nitrogen deposition, increased temperature and management on carbon sequestration in temperate and boreal forest ecosystems: A literature review. *New Phytol.* **2007**, *173*, 463–480. [[CrossRef](#)] [[PubMed](#)]
51. Drake, B.G.; Gonzalez-Meier, M.A.; Long, S.P. More efficient plants: A consequence of rising atmospheric  $\text{CO}_2$ ? *Annu. Rev. Plant Physiol. Plant Mol. Biol.* **1997**, *48*, 609–639. [[CrossRef](#)]
52. Battipaglia, G.; Saurer, M.; Cherubini, P.; Calfapietra, C.; McCarthy, H.R.; Norby, R.J.; Cotrufo, M.F. Elevated  $\text{CO}_2$  increases tree-level intrinsic water-use efficiency. Insights from carbon and oxygen isotopes analyses in tree rings across three forest FACE sites. *New Phytol.* **2013**, *197*, 544–554. [[CrossRef](#)] [[PubMed](#)]
53. Giammarchi, F.; Cherubini, P.; Pretzsch, H.; Tonon, G. The increase of atmospheric  $\text{CO}_2$  affects growth potential and intrinsic water-use efficiency of Norway spruce forests: Insights from a multiple-stable isotope analysis in tree rings of two Alpine chronosequences. *Trees* **2017**, *31*, 503–515. [[CrossRef](#)]
54. Wullschleger, S.D.; Tschaplinski, T.J.; Norby, R.J. Plant water relations at elevated  $\text{CO}_2$ —Implications for water-limited environments. *Plant Cell Environ.* **2002**, *25*, 319–331. [[CrossRef](#)] [[PubMed](#)]
55. Cao, L.; Yan, Z.; Zhao, P.; Zhu, Y.; Yu, Y.; Tang, G.; Jones, P. Climatic warming in China during 1901–2015 based on an extended dataset of instrumental temperature records. *Environ. Res. Lett.* **2012**, *12*, 064005. [[CrossRef](#)]
56. Qin, J.; Yang, K.; Liang, S.; Guo, X. The altitudinal dependence of recent rapid warming over the Tibetan plateau. *Clim. Chang.* **2009**, *97*, 321–327. [[CrossRef](#)]
57. Altieri, S.; Mereu, S.; Cherubini, P.; Castaldi, S.; Sirignano, C.; Lubritto, C.; Battipaglia, G. Tree-ring carbon and oxygen isotopes indicate different water-use strategies in three Mediterranean shrubs at Capo caccia (Sardinia, Italy). *Trees* **2015**, *29*, 1593–1603. [[CrossRef](#)]
58. Xu, G.; Liu, X.; Qin, D.; Chen, T.; An, W.; Wang, W.; Wu, G.; Zeng, X.; Ren, J. Climate warming and increasing atmospheric  $\text{CO}_2$  have contributed to increased water use efficiency on the northeastern Tibetan plateau since 1850. *Trees Struct. Funct.* **2013**, *27*, 465–475. [[CrossRef](#)]
59. Hietz, P.; Wanek, W.; Duenisch, O. Long-term trends in cellulose delta C-13 and water-use efficiency of tropical Cedrela and Swietenia from Brazil. *Tree Physiol.* **2005**, *25*, 745–752. [[CrossRef](#)] [[PubMed](#)]
60. Wils, T.H.G.; Roberston, I.; Woodborne, S.; Hall, G.; Kaprowski, M.; Eshetu, Z. Anthropogenic forcing increases the water-use efficiency of African trees. *J. Quat. Sci.* **2016**, *31*, 386–390. [[CrossRef](#)]
61. Urrutia-Jalabert, R.; Malhi, Y.; Barichivivh, J.; Lara, A.; Delgado-Huertas, A.; Rodríguez, C.G.; Cuq, E. Increased water use efficiency but contrasting tree growth patterns in *Fitzroya cupressoides* forests of southern Chile during recent decades. *J. Geophys. Res. Biogeosciences* **2015**, *120*, 2505–2524. [[CrossRef](#)]
62. Keenan, T.F.; Hollinger, D.Y.; Bohrer, G.; Dragoni, D.; Munger, J.W.; Peter, H. Richardson, Increase in forest water-use efficiency as atmospheric carbon dioxide concentrations rise. *Nature* **2013**, *499*, 324–327. [[CrossRef](#)]
63. Feng, X. Trends in intrinsic water-use efficiency of natural trees for the past 100–200 years: A response to atmospheric  $\text{CO}_2$  concentration. *Geochim. Cosmochim. Acta* **1999**, *63*, 1891–1903. [[CrossRef](#)]
64. Penuelas, J.; Hunt, J.M.; Ogaya, R.; Jump, A.S. Twentieth century changes of tree ring  $\delta^{13}\text{C}$  at the southern range-edge of *Fagus sylvatica*: Increasing water use efficiency does not avoid the growth decline induced by warming at low altitudes. *Glob. Chang. Biol.* **2008**, *14*, 1076–1088. [[CrossRef](#)]

65. Frank, D.; Poulter, B.; Saurer, M.; Esper, J.; Huntingford, C.; Helle, G.; Treydte, K.; Zimmermann, N.E.; Schleser, G.H.; Ahlström, A.; et al. Water-use efficiency and transpiration across European forests during the Anthropocene. *Nat. Clim. Chang.* **2015**, *5*, 579–583. [[CrossRef](#)]
66. Silva, L.C.R.; Anand, M.; Oliveira, J.M.; Pillar, V.D. Past century changes in *Araucaria angustifolia* (Bertol.) Kuntze water use efficiency and growth in forest and grassland ecosystems of southern Brazil: Implications for forest expansion. *Glob. Chang. Biol.* **2009**, *15*, 2387–2396. [[CrossRef](#)]



© 2019 by the authors. Licensee MDPI, Basel, Switzerland. This article is an open access article distributed under the terms and conditions of the Creative Commons Attribution (CC BY) license (<http://creativecommons.org/licenses/by/4.0/>).